Catalysis Today 166 (2011) 159–165

Contents lists available at ScienceDirect

Catalysis Today

journal homepage: www.elsevier.com/locate/cattod

# Photophysical and photocatalytic properties of $TiO_2$-Cr sol–gel prepared semiconductors

R. López [a,*], R. Gómez [a], S. Oros-Ruiz [b]

[a] Universidad Autónoma Metropolitana-Iztapalapa, Departamento de Química, ECOCATAL, Av. San Rafael Atlixco No. 186, C.P. 09340, México, DF, Mexico
[b] Doctorado Institucional en Ingeniería y Ciencia de Materiales, Universidad Autónoma de San Luis Potosí, Av. Manuel Nava No. 6, Zona Universitaria, San Luis Potosí, SLP, Mexico

ARTICLE INFO

*Article history:*
Available online 1 February 2011

*Keywords:*
Photocatalysts
Sol–gel
Phenol photodegradation
Chromium–titania photo catalysts
XPS chromium–titania
UV–vis chromium–titania spectra

ABSTRACT

Chromium–titania photocatalysts were prepared at different contents in chromium oxide (0.1–5.0 wt.%) by gelling titanium alkoxide and chromium nitrate. Nanostructured titania with crystallite sizes between 22 and 40 nm and high specific surface areas (68–113 $m^2/g$) were obtained in solids annealed at 500 °C. The determination of the band gap energy showed a shift to the visible region in samples containing high amounts of chromium oxide (3.8–1.8 eV). XPS spectroscopy evidenced the presence of Cr(III) and Cr(VI) in the annealed semiconductors. The photocatalyst with low doping content (0.1 wt.% Cr) was observed to provide effective Cr–Ti interaction and allow the maximum photoactivity.



## 1. Introduction

Titanium dioxide has been widely studied and its applications have been improved by different research centers throughout the world. The wide applications of this important semiconductor include optical coatings, solar energy conversion, gas sensing, water splitting, photo voltaic devices and pollutant destruction [1–5]. Several methods, including the effective incorporation of doping cations like transition metals into $TiO_2$ network, have been employed to improve the photophysical properties of $TiO_2$. Among the methods that have been reported for successful incorporation of dopants into $TiO_2$, the following can be mentioned: plasma spraying, anodization, thermal oxidation and chemical vapor deposition [6]. Most of the above referred techniques are complicated and require the use of expensive apparatus. In this way, the sol–gel process seems to be an easy and effective method to incorporate dopants into the $TiO_2$ lattice [7]. When doping is used for photocatalytic purposes, the incorporation of transition metals such as Fe, Mo, Cu, Ni [8–10] has been reported as a good doping alternative. Among doping transition metals chromium has been reported as a very effective $TiO_2$ doping metal, which notably improves the photoactivity for the oxidizing decomposition of Rhodamine B [11], methylene blue [12,13], azoic dye active yellow XRG [14], oxalic acid, propene and 2-propanol [15] among others. However, it has also been reported that the use of chromium has a detrimental effect on photoactivity [16–18]. The negative effect of chromium on photoactivity was related by Herrmann et al. [18] to the role of Cr(III) by inducing a fast electron–hole recombination. Extensive characterization of $Cr/TiO_2$ semiconductors has been reported in solids prepared by very different methods. For instance, in $Cr/TiO_2$ P-25 chromium has been found as a complex mixture of Cr(III), Cr(V) and Cr(VI) [19], whereas in titania films prepared by the sol–gel method only the presence of Cr(III) has been observed by XPS spectroscopy [20]. Furthermore, when the catalysts were prepared by hydrothermal doping of $TiO_2$, the presence of Cr(III) and Cr(IV) was also observed [14]. According to the information available in the literature, the role of the chrome oxidation and its positive or negative effect on titania Cr-doped semiconductors for photocatalytic purposes is still a controversial subject.

With the aim of understanding the role of chromium as a doping agent, we have studied the $TiO_2$-Cr photocatalysts. Since the cationic radius of Cr(III) (0.69 Å) is comparable to that of Ti (IV) (0.68 Å); therefore, a possible substitution of Ti(IV) in the titania framework can be achieved. The Cr-doped $TiO_2$ semiconductors were synthesized by the sol–gel method using as starting precursors chromium nitrate and titanium butoxide. The synthesized materials were characterized by nitrogen adsorption, UV–vis and FTIR spectroscopy, X-ray diffraction, X-ray photoelectronic spectroscopy and thermal analysis. The photocatalytic evaluation was made for the phenol photodegradation under UV light source. In order to know the extent of the photodegradation, the analysis of total organic carbon in the irradiated solution was made.

* Corresponding author. Tel.: +52 55 58044668; fax: +52 55 58044666.
*E-mail addresses:* ross@xanum.uam.mx (R. López), gomr@xanum.uam.mx (R. Gómez), coco.oros@hotmail.com (S. Oros-Ruiz).

0920-5861/$ – see front matter © 2011 Elsevier B.V. All rights reserved.
doi:10.1016/j.cattod.2011.01.010

## 2. Experimental

### 2.1. Materials and reagents

The following reagents were used as received without purification for the preparation of the $TiO_2$-Cr semiconductors: titanium (IV) butoxide (Aldrich 97%), chromium (III) nitrate nonahydrate (Aldrich 99.99%), 1-butanol (Aldrich 99.4%), nitric acid (Aldrich), phenol (Mallinckrodt) and distilled-deionized water (18 MΩ cm).

### 2.2. Synthesis

The photocatalysts, $TiO_2$ and $TiO_2$-Cr (0.1, 0.5, 1.0 and 5.0 wt.% of Chromium) were synthesized by the sol–gel method. An appropriated amount of chromium (III) nitrate nonahydrate, which was calculated to obtain the desired Cr content in the material (0.196, 0.971, 1.96, 9.81 mmol for the 0.1, 0.5, 1.0 and 5.0 wt.% of chromium, respectively), was added to a flask containing 18 mL of distilled-deionized water, 44 mL of 1-butanol and 0.2 mL of nitric acid (to obtain pH 3). Subsequently, 44 mL of titanium (IV) butoxide were added drop wise to the solution during 4 h (water/alkoxide molar ratio of 8). The gelling solution was then heated at 70 °C under reflux and maintained under constant stirring for 24 h until the gel was formed. The obtained xerogels were dried at 70 °C for 24 h. The dried solids were ground in an agate mortar until a fine and homogeneous powder mixture was obtained. Finally, the solids were annealed in air at 500 °C for 4 h, using a heating rate of 2 °C/min. As a reference, undoped $TiO_2$ sol–gel sample was prepared according to the protocol described above without the addition of the corresponding chromium precursor.

### 2.3. Photocatalyst characterization

The specific surface area of the solids were determined by nitrogen adsorption isotherms obtained with a Quantachrome Autosorb-3B apparatus; this equipment has the ability to apply multiple methods of analyses at the same time, such as multipoint BET and BJH methods (pore size distribution). Before adsorption, the samples were desorbed in vacuum at 300 °C overnight. The pore size distribution was calculated using the branch of desorption from the isotherm, by applying the BJH method. The fractal dimension, which describes the topography of a real surface in terms of a "roughness exponent", is known as fractal dimension D. It was estimated from the adsorption–desorption isotherms data applying the Frenkel–Halsey–Hill equation expressed as

$$\ln(S^{1g}) = \text{const} - (3 - D_s)\ln(\mu)$$

where $S^{lg}$ is the amount adsorbed at the relative pressure $P/P^o$ and $\mu$ is the called adsorption potential defined as [21,22]:

$$\mu = RT\ln\left(\frac{P^o}{P}\right)$$

Many real surfaces have surface irregularities that appear to be similar at different scales, assuming values between $D = 2$ (for smooth surfaces) and $D = 3$ (for extremely rough surfaces that they essentially occupy all available volume). The fractal dimension D quantifies the roughness of real surfaces in terms of a single parameter [23]. In order to estimate the possible electronic transitions and the energy band gap ($E_g$) of the semiconductors, a Cary 100 Scan spectrophotometer (Varian) equipped with an integrating sphere (Labsphere DRA-CA-30I) was used. The equipment was calibrated with a Spectralon standard (Labsphere SRS-99-010, 99% reflectance). The obtained diffuse reflectance spectrum was transformed to a magnitude proportional to the extinction coefficient ($\alpha$) through the Kubelka–Munk (K–M) function:

$$F(R) = \frac{(1-R)^2}{2R}$$

where $R$ is the reflectance and $F(R)$ is the Kubelka–Munk function. Then, the $E_g$ was estimated from the plot of the modified K–M, $[F(R)xh\nu]^{1/2}$ vs energy of the absorbed light for indirect allowed transitions. Fourier Transform Infrared Spectra were recorded in a Shimadzu IRAffinity-1 equipped with ATR module. The measurements were conducted in an absorbance mode within the frequency range of 4000–350 $cm^{-1}$, with a resolution of 2 $cm^{-1}$. The samples were mixed with KBr at 5 wt.%. The X-ray powder diffraction (XRD) patterns were collected at room temperature using a Siemens D-500 diffractometer operated at 40 kV and 30 mA. The Cu Kα radiation was selected using a graphite monochromator. The measurements were recorded in steps of 0.03° with a count time of 1 s in the $2\theta$ range from 5 to 70°. The average anatase crystallite size was determined by the Scherrer formula ($D = K\lambda/\beta\cos\theta$), where $D$ is the crystallite size, $K$ is a constant equal to 0.94, $\lambda$ is the wavelength (1.5405 Å), $\theta$ is the diffraction angle and $\beta$ is the full width at half maximum (FWHM) of the XRD peak. In order to analyze the oxidation state of the doping metal in the titania semiconductors, X-ray photoelectron spectroscopy (XPS) was used. The electron spectrometer was a Thermo VG Scientific ESCALAB 250 equipped with hemispherical analyzer equipment. The operating conditions of the spectrometer were put at constant pass energy mode and monochromatized Al Kα radiation ($h\nu = 1486.6$ eV) was used. The X-ray source operated at 10 mA and 15 kV. The peaks intensities were estimated by calculating the integral of each peak after subtracting the S-shaped background and fitting the experimental peak with a combination of Lorentzian/Gaussian lines of variable proportions. The binding energies (BE) were referenced to the C (1s) peak, which was fixed at 284.6 eV. The thermal analysis was done in a STA i1000 simultaneous thermal analyzer using a heat rate of 10 °C $min^{-1}$ and a $N_2$ flux of 10 $cm^3$ $min^{-1}$.

### 2.4. Photocatalytic test

To prove the efficiency of the prepared photocatalyst, the activity of the samples was evaluated in phenol oxidation. The photocatalytic reaction was carried out in a glass reactor containing 200 ml of aqueous solution with 30 ppm of organic molecule and 0.2 g of photocatalyst. The powder suspension was stirred and irradiated with a high pressure mercury lamp (UV lamp, emitting at 254 nm, 2.16 watts, 18 mA) protected with a quartz tube and immersed in the center of vessel. To assure the adsorption–desorption equilibrium of the molecule in the solution, the suspension was stirred for 30 min in the dark with an air flow of 2 ml/s (Air-Pump BOYU S-4000B); then, the solution was irradiated with the UV lamp (Pen-Ray UVP). The pH of the initial solution was 6 with no variations in the irradiated solution (3 h under irradiation). The degradation of the pollutant was monitored by collecting samples at 20 min intervals and following the main section of the phenol absorption band at 268 nm with a UV–vis spectrophotometer Varian Cary 100 UV–vis. To avoid interferences in the UV–vis analysis associated with suspended solids, each sample was filtered through a nylon membrane (0.45 μm, Millipore) to remove the oxide particles before analysis. To determine the mineralization achieved, total organic carbon (TOC) measurements were carried out with a Shimadzu TOC-V CPN (equipped with a NDIR detector). The respective probes for possible Cr leaching in the reactant medium (see Standard Methods for the Examination of Water and Wastewater, 20th edition, pp. 3–65, American Public Health Association, Washington, DC, 1998) do not show any con-

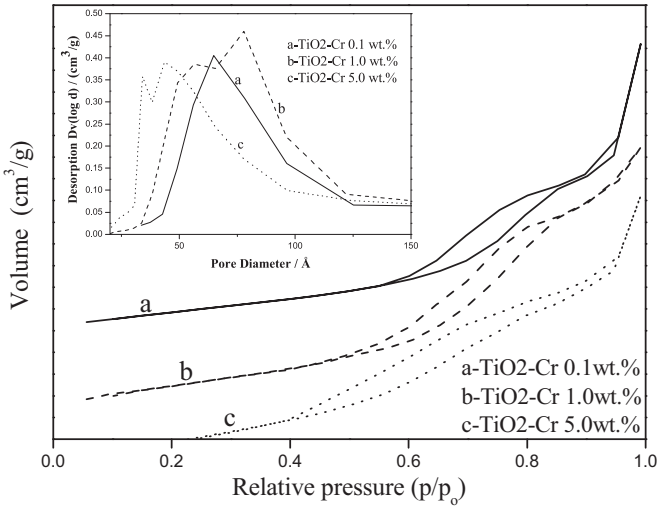


**Fig. 1.** Nitrogen adsorption isotherms for selected $TiO_2$-Cr samples.

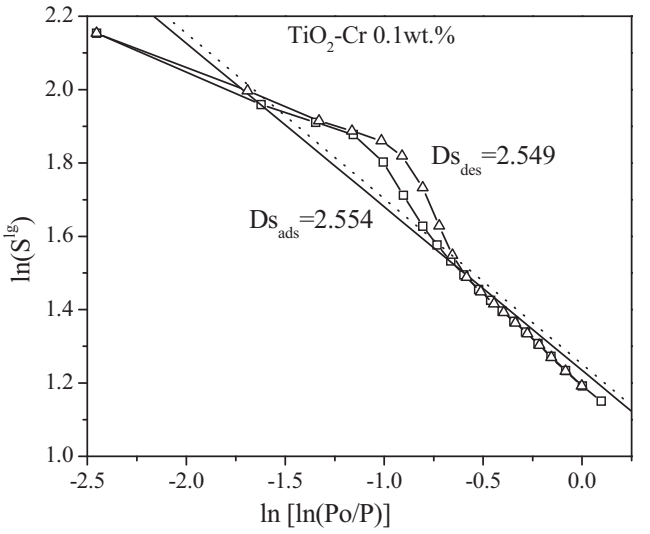


**Fig. 2.** The Frenkel–Halsey–Hill fractal analysis of the isotherms for the $TiO_2$-Cr 0.1 wt.%.

tent of chromium dissolved in media. The sensitivity of the method is 0.1 ppm.

## 3. Results and discussion

### 3.1. Nitrogen adsorption and fractal analysis

Nitrogen adsorption–desorption isotherms and pore size distributions of selected photocatalyst are shown in Fig. 1, They correspond to type IV, which is characteristic of mesoporous materials [24] and present an H1 type hysteresis loop according to IUPAC classification. At low doping content (0.1 and 0.5%) in the samples, the pore size distribution (insert in Fig. 1) shows a monomodal distribution. When the Cr content increases to 1.0 wt.%, a bimodal pore size distribution can be observed. This kind of distribution arises at the highest doping content (5.0 wt.%), where it is clearly observed the bimodal distribution possibly attributed to the superficial formation of chromium oxides as conglomerates. The results of the specific surface areas, pore volume and pore size distribution were summarized in Table 1, where their specific surface area is observed to increase with the doping content. In heterogeneous catalysis usually a high specific surface area promotes a faster oxidation of organic molecules, however for photocatalytic heterogeneous reactions it seems that the surface area effects are of minor importance in comparison to other photophysical properties such as the abundance of crystalline phases, $E_g$, etc. In the present study, as can be seen in Table 1, the specific surface area effect on the photoactivity is of minor importance, since the 5.0 wt.% Cr photocatalyst (113 $m^2$/g) is less active than the 0.1 wt.% Cr (68 $m^2$/g). Therefore, other factors then, such as chromium oxidation state or crystallite size, must be taken into consideration in order to explain enhancements in photoactivity. The fractal dimension, $D_s$, is indicative of a solid capacity for adsorption and permeability; also, it can be considered an important characteristic of the smoothness or roughness of solids. The fractal dimension can be directly related to the wrinkled level on the surface area of $TiO_2$ and $TiO_2$-Cr semiconductors [25]. As an example of the Frenkel–Halsey–Hill treatment of the adsorption–desorption isotherms, Fig. 2 shows the $D_s$ for 0.1 wt.%, the corresponding values obtained for the samples are reported in Table 1. From the $D_s$ values, fractal surface of the material can be assumed [26]. The values of Table 1 show that the fractal dimension is sensitive to the chromium content. At 0.5 wt.% the fractal geometry is almost the same than that for the pure $TiO_2$ structure. The $D_s$ values are between 2.47 and 2.65, the lowest values imply that the pore walls were smooth, whereas the highest values indicate a greater roughness of the surface. The sample with the highest roughness showed the highest specific surface area (113 $m^2$/g).

### 3.2. UV–vis diffuse reflectance spectroscopy

The calculated $E_g$ values are reported in Table 1, where the energy band gap is seen to diminish from 3.18 to 1.80 eV for low and high chromium oxide content in the samples, respectively [27]. The red shift of the adsorption edge has been attributed to the localized states near the conduction or valence band of the modified semiconductors [28]. It has also been attributed to the formation of color centers, which were associated with the oxygen vacancies in pure $TiO_2$ or to the radicals in the titanium dioxide lattice associated with the doping ions [29]. Our assumption is that at high doping levels as 5.0 wt.%, an excess of the chromium precursor is present. The formation of chromium oxide clusters on the surface of the $TiO_2$ is expected [30] and these are responsible for the light absorption in the visible region. The spectra (not shown [27]) are typical of $O^{2-}(2p) \rightarrow Ti^{4+}(3d)$ transitions in the tetrahedral symmetry of $TiO_2$ [31]. An absorption band situated in the visible region is also present (~700 nm) and is attributed to the $^4A_{2g} \rightarrow {}^4T_{2g}$ d–d of $Cr^{3+}$ [17]. The $TiO_2$-Cr powders with a doping content of 0.1, 0.5 and 1.0 wt.% are yellow-orange colored, whereas the powder with a doping content of 5.0 wt.% is a dark-green colored sample [32].

**Table 1**
Specific surface area, pore volume and mean pore size distribution, fractal dimension and energy band gap for the $TiO_2$-Cr photocatalysts.

| Doping (wt.%) | Specific surface area ($m^2$/g) | Pore volume ($cm^3$/g) | Pore size (Å) | Fractal dimension | $E_g$ (eV) |
|---|---|---|---|---|---|
| 0.1 | 68 | 0.21 | 65 | 2.549 | 3.16 |
| 0.5 | 78 | 0.31 | 97 | 2.479 | 3.06 |
| 1.0 | 99 | 0.21 | 49 | 2.624 | 3.04 |
| 5.0 | 113 | 0.22 | 34 | 2.651 | 1.80 |
| Pure | 72 | 0.33 | 95 | 2.467 | 3.18 |

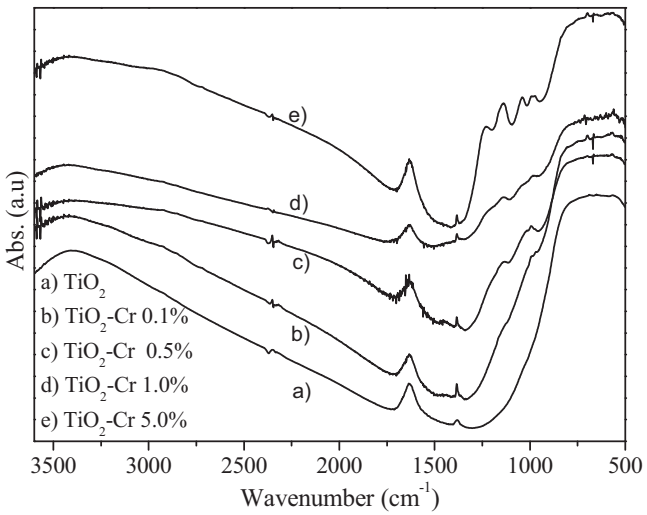


**Fig. 3.** FTIR spectra for the $TiO_2$-Cr solids annealed at 500 °C, (a) $TiO_2$, (b) 0.1 wt.%, (c) 0.5 wt.%, (d) 1.0 wt.% and (e) 5.0 wt.%.

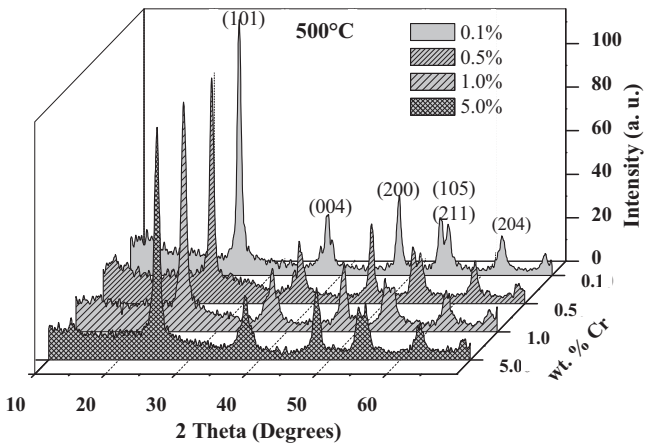


**Fig. 4.** X-ray diffraction patterns of the $TiO_2$-Cr materials annealed at 500 °C.

This change in color indicates a variation in the Cr(III)/Cr(VI) ratio. The Cr (III) in the precursor nitrate was partially oxidized to Cr(VI).

### 3.3. Fourier transform infrared spectroscopy

To analyze the structure of the materials the FTIR spectra of $TiO_2$-Cr were taken (Fig. 3). The 450–750 $cm^{-1}$ region is typical of $TiO_2$ anatase structure vibration; these low-energy bands were related to the stretching vibration of the Ti–O and Ti–O–Ti bonds. At 1630 $cm^{-1}$ the typical vibration frequency is observed due to the OH bending vibration band of physically adsorbed water in the xerogels; the intensity of this signal does not vary significantly with the increase in Cr content. The broad band centered at 3450 $cm^{-1}$ is attributed to the enlargement vibration of the interacting hydroxyl groups coordinated with $Ti^{4+}$ cations ($Ti^{4+}$-OH) and can also be attributed to the surface of adsorbed water molecules and surface adsorbed hydroxyl groups [33–35].

### 3.4. Crystalline titania phase identification

The diffractograms for the $TiO_2$-Cr annealed at 500 °C showed that the presence of Cr in $TiO_2$ preserves the anatase crystalline phase (JCPDS 21-1272), and no rutile peaks are observed at any Cr doping content, Fig. 4. The diffraction patterns of the samples do not show the formation of chromium titanates such as $Cr_2TiO_5$ (at 34.11 2$\theta$, JCPDS 33-0409) or $CrTiO_3$ (at 54.62 2$\theta$, int. 100, JCPDS 33-0408). Chromium oxide reflections associated with $Cr_2O_3$ (at 36.19 2$\theta$, JCPDS 04-0765) are not observed suggesting the insertion of chromium cations in the titania network or the formation on the titania surface of highly dispersed chromium oxide conglomerates. According to the Goldschmidt's rules in a crystalline solid, the ions substitution occurs only if the difference in the atomic ratio is lower than 15%. Therefore, $Ti^{4+}$ (0.68 Å) can be successfully substituted only by $Cr^{3+}$ (0.69 Å), for which reason the incorporation of Cr into the $TiO_2$ lattice causes soft modifications in the lattice parameters and crystallite size, Table 2. The crystallite size was estimated from the FWHM of the (1 0 1) and (2 0 0) planes of anatase using the Scherrer equation. The crystallite size decreases as a function of Cr content. The results show nanostructured materials from 22 to 40 nm. The values obtained for the lattice parameters and unit cell volume showed unpredictable behavior and the values are listed for comparative studies.

### 3.5. X-ray photoelectron spectroscopy

To evaluate the interaction between chromium and titanium dioxide, the chromium oxidation state was analyzed by XPS spectroscopy [9,36–38]. All complete spectra (survey) were calibrated at the C 1s peak (284.5 eV) that corresponds to carbon and is always present on the surface of the powdered samples (adventitious carbon). The Ti 2p peak (not shown) for each sample was situated at the binding energy of 458.6 eV. The Cr 2p core level binding energy signal was deconvoluted and is present in Fig. 5. The deconvoluted XPS spectra indicate that mixed oxidation states of chromium are present in the doped materials. The initial precursor Cr(III) oxidation state was in part modified by the experimental procedure. The Cr $2p_{3/2}$ binding energy (BE) corresponding to Cr(III) and Cr(VI) is 576.6 eV and 578.6 eV, respectively and (being of the same order) it shows similar values for all the samples with a variation of about 0.1 eV (Table 3). The energy difference between Cr $2p_{3/2}$ and Cr $2p_{1/2}$ was approximately 9.6 eV and it is constant for all doping contents [39]. The integral area under Cr(III) and Cr(VI) peaks reveal that Cr(III) is the predominant species (60% approx.). As expected, the

**Table 2**
Structural parameters for the $TiO_2$-Cr doped materials.

| Photocatalyst | 2$\theta$ | $d_{hkl}$ | Unit cell volume (Å)$^3$ | Lattice parameters (Å) | Crystallite size (nm) |
|---|---|---|---|---|---|
| $TiO_2$ | 25.436 | 3.498 | 132.244 | $a = b = 3.779$, $c = 9.259$ | 40.5 |
| | 48.116 | 1.889 | | | |
| $TiO_2$-Cr 0.1% | 25.466 | 3.494 | 132.419 | $a = b = 3.770$, $c = 9.315$ | 31.83 |
| | 48.236 | 1.885 | | | |
| $TiO_2$-Cr 0.5% | 25.436 | 3.498 | 133.196 | $a = b = 3.772$, $c = 9.359$ | 30.18 |
| | 48.206 | 1.886 | | | |
| $TiO_2$-Cr 1.0% | 25.436 | 3.498 | 131.332 | $a = b = 3.785$, $c = 9.163$ | 24.37 |
| | 48.026 | 1.892 | | | |
| $TiO_2$-Cr 5.0% | 25.406 | 3.502 | 134.314 | $a = b = 3.772$, $c = 9.437$ | 22.52 |
| | 48.206 | 1.886 | | | |

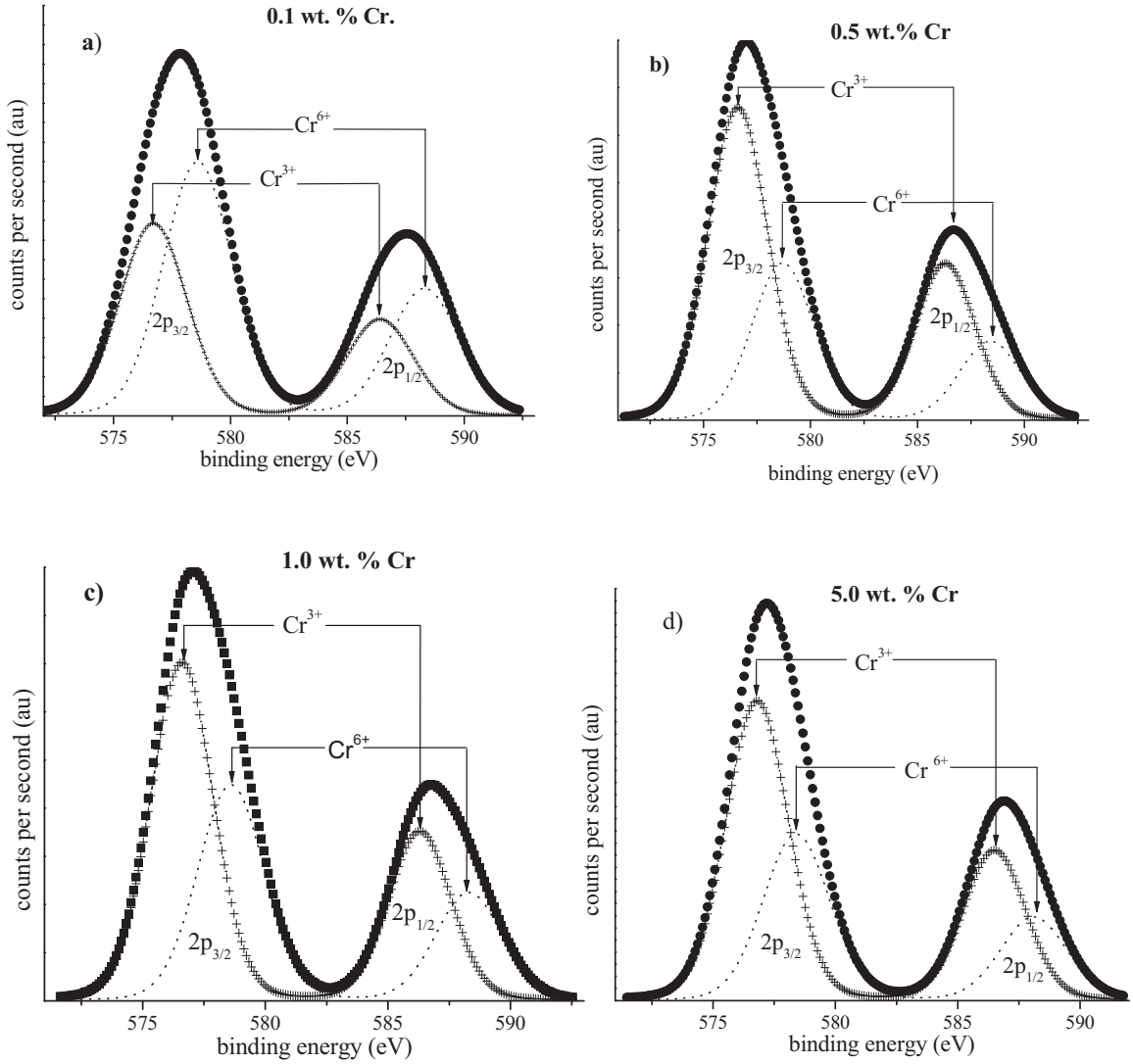


**Fig. 5.** X-ray photoelectron spectra; deconvolution of the Cr $2p_{3/2}$ and Cr$2p_{1/2}$ peaks, (a) 0.1 wt.%, (b) 0.5 wt.%, (c) 1.0 wt.% and (d) 5.0 wt.%.

Cr/Ti ratio increases with the doping content and the highest value was 0.144 for the 5 Cr wt.%. In the survey spectra the O 1s signal can be observed; the deconvoluted signal shows two contributions (not shown), the first located around 529–530 eV (Table 3) which corresponds to the Ti–O bonds in the $TiO_2$ lattice (the corresponding percentages are in parenthesis), whereas the second peak on deconvoluted spectra (531.5 eV) is attributed to Ti-OH hydroxyl groups arising from the synthesis method [40]. It can be observed that the O 1s signal intensity increases as chromium content increases.

**Table 3**
Binding energies of core electrons, valences, intensities and surface atomic ratios of Cr/$TiO_2$ catalysts.

| Sample (wt.%) | Cr $2p_{3/2}$ (eV) | | O 1s | Surface atomic ratio |
|---|---|---|---|---|
| 500 °C | BE (%)[a] | FWHM | BE (%)[b] | Cr/Ti |
| $TiO_2$-Cr (0.1) | 576.6 (59) | 4.288 | 530.0 (86) | 0.009 |
| | 578.6 (41) | | 531.5 (14) | |
| $TiO_2$-Cr (0.5) | 576.7 (66) | 3.975 | 529.9 (84) | 0.037 |
| | 578.7 (34) | | 531.5 (16) | |
| $TiO_2$-Cr (1.0) | 576.6 (59) | 3.840 | 530.0 (87) | 0.053 |
| | 578.6 (41) | | 531.6 (13) | |
| $TiO_2$-Cr (5.0) | 576.7 (60) | 3.552 | 529.9 (88) | 0.144 |
| | 578.5 (40) | | 531.4 (12) | |

[a] The percent values correspond to Cr(III) and Cr(VI).
[b] The percent values correspond to Ti–O and Ti-OH.

### 3.6. Thermal analysis

A simultaneous differential scanning calorimetry (DSC) and thermogravimetric analysis (TGA) were done in the doped and undoped xerogels dried at 70 °C for 24 h. In Fig. 6 TGA and DSC (insert on graph) analyses were plotted for the selected samples of $TiO_2$-Cr 0.1, $TiO_2$-Cr 1.0 wt.% and pure S-G $TiO_2$. In all samples two principal weight losses can be identified. The first located between 25 and 260 °C corresponds to a loss of 13% approximately, associated with the evaporation of physically adsorbed water and remaining nitrates. The second one was located between 260 and 500 °C which corresponds to the remaining precursor combustion and structural water ($OH^-$) [41]. Simultaneously, from DSC analysis, the exothermic peak at about 265 °C was also attributed to the combustion of remaining chromium nitrates and the formation of chromium oxides ($CrO_3$ and $Cr_2O_3$) [42]. The second exothermic peak at about 416 °C corresponds to the transformation of amorphous titania to the anatase phase and is sharper for the pure $TiO_2$. For a low doping content (0.1 wt.%), the DSC curve indicates that crystallization to anatase phase was modified by the substitution of Ti(IV) by Cr(III).

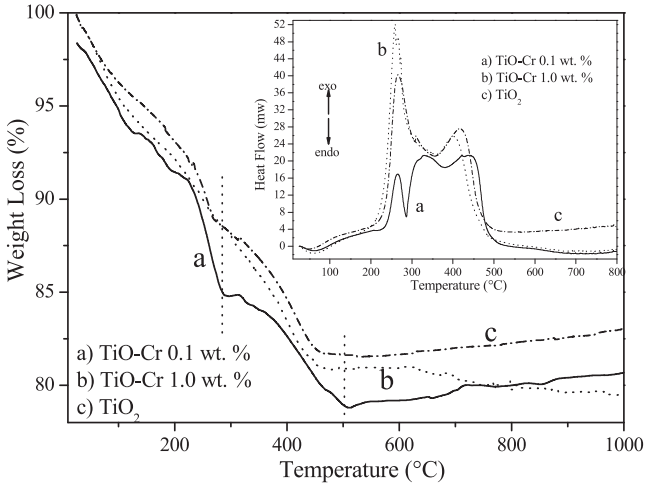


**Fig. 6.** TGA and DSC (insert) plots for (a) $TiO_2$-Cr 0.1 wt.%, (b) $TiO_2$-Cr 1.0 wt.% and (c) $TiO_2$.

### 3.7. Photocatalysis

The photocatalytic activity for the various solids is shown in Fig. 7 as phenol oxidized vs time. The formation of hydroquinone, catechol and p-benzoquinone has been reported as intermediates for the phenol photooxidation and their concentration as a function of time under UV irradiation of phenolic solutions is lower than 5%. So, this low concentration of intermediates allows us to consider that the phenol signal analyzed by UV–vis spectroscopy is only slightly perturbed by the presence of these intermediates [43]. In Fig. 7 it can be seen that 38–42% of phenol was oxidized after 4 h under reaction on 0.5, 1.0 and 5.0 wt.% Cr photocatalysts, whereas for $TiO_2$-Cr (0.1 wt.% Cr) and for the undoped $TiO_2$ the photodegradation arises to 95 and 70%, respectively. Photocatalytic degradation of organic contaminants usually follows a pseudo-first order kinetics [44,45] and for the phenol decomposition the pseudo first order rate constant was obtained (Fig. 8). The calculated value of the rate constant was $2.8 \pm 0.6 \times 10^{-3}$ $min^{-1}$ for the photocatalysts with 0.5, 1.0 and 5.0 wt.% Cr (around 40% of phenol oxidized) and it showed that for doping contents higher than 1.0% the photoactivity was not significantly modified. On the other hand, the rate constants for $TiO_2$ and Cr 0.1 wt.% were $5.5 \times 10^{-3}$ and $10.1 \times 10^{-3}$ $min^{-1}$ respectively (Fig. 8). The photocatalysts of doped

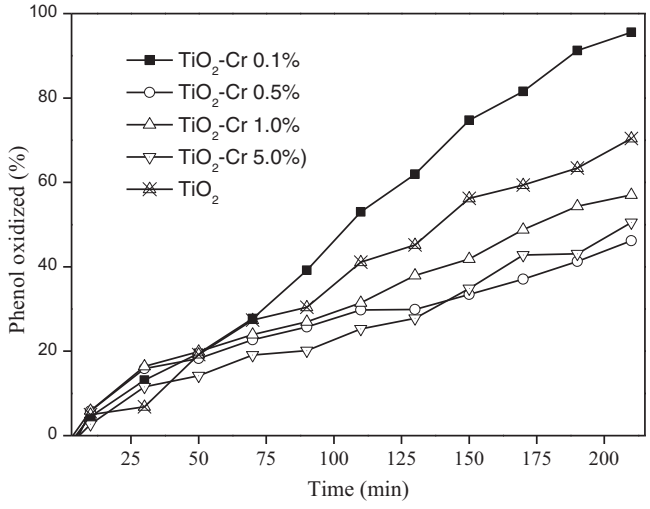


**Fig. 7.** Photocatalytic activity for the phenol decomposition as a function of time.

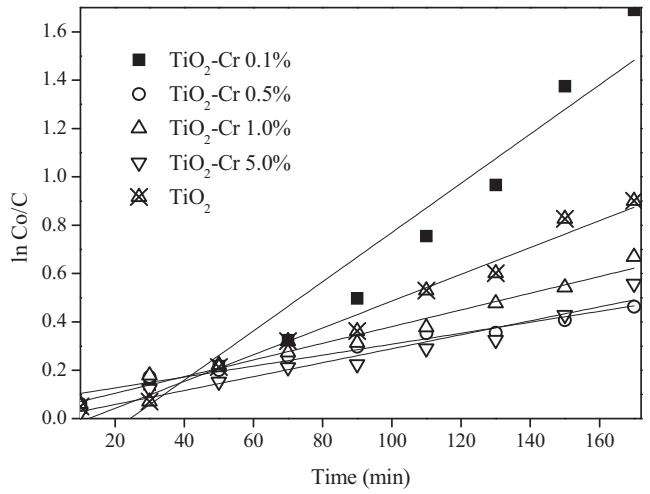


**Fig. 8.** Pseudo first order kinetics for the phenol photodegradation for Cr-doped $TiO_2$ semiconductors.

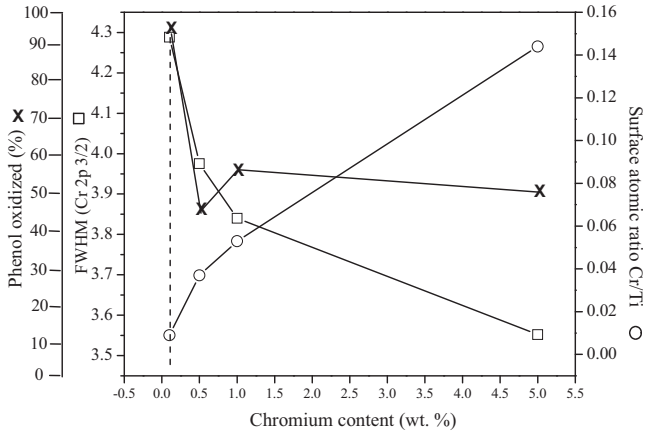


**Fig. 9.** Effect of the overall XPS signal intensity (FWHM), chromium content and photocatalytic activity as a function of the chromium content.

titania with the lowest Cr content double the photoactivity presented by the bare $TiO_2$. This indicates that an effective reduction in the electrons and hole recombination rate could be achieved with photocatalysts at low doping contents. It is worth mentioning that the role of Cr(III) and Cr(VI) in photoactivity was well established in the present study and we consider that the overall XPS signal intensity (FWHM) can be related to the photoactivity enhancement (Fig. 9). Table 3 shows that the lowest Cr/Ti ratio corresponds to the $TiO_2$/Cr 0.1 wt.% catalyst, thus in this catalyst a higher Cr–Ti interaction was obtained and hence the positive effect of Cr on retarding the electron–hole is magnified. To ensure that the phenol photooxidation was achieved, the determination of the total organic carbon in the reactant solution was made. The obtained values showed that the initial phenol concentration (TOC) was reduced in $60 \pm 5\%$ for the catalysts with chromium contents of 0.5, 1.0 and 5.0 wt.%. For the bare $TiO_2$, TOC reduction was 70% and for the doped catalyst with 0.1 wt.% Cr it was 90%.

## 4. Conclusions

It is shown that by gelling titanium alkoxide in the presence of chromium nitrate, $TiO_2$-Cr photocatalysts with high specific surface area and nanostructured crystalline structure are obtained. A shift in the band gap energy to the visible region is produced in the chromium doped-$TiO_2$ photocatalysts in comparison to the

$TiO_2$ bare catalyst. The modification of the initial chromium oxidation state Cr (III) to Cr (VI) occurring during the annealing of the solids was evidenced by XPS spectroscopy. It is shown that with the photocatalyst at low doping content (0.1 wt.% Cr) an effective Cr–Ti interaction was obtained and a maximum photoactivity was reached.

## Acknowledgements

R. López and S. Oros-Ruíz acknowledge the scholarship given by CONACYT México. We thank to CONACYT for the CB-2006-1-62053 grant relative to: "Preparation of semiconductors by the sol–gel method".

## References

[1] D. Niemeyer, D. e. Williams, P. Smith, K.F.E. Pratt, B. Slater, C.R.A. Catlow, A.M. Stoneham, J. Mater. Chem. 12 (2002) 667.
[2] I.N. Kholmanov, E. Barborini, S. Vinati, P. Piseri, A. Podesta, C. Ducati, C. Lenardi, P. Milani, Nanotechnology 14 (2003) 1168.
[3] J.R. Bolton, S.J. Strickler, J.S. Connolly, Nature 316 (1985) 495.
[4] A.L. Linsebigler, G. Lu, J.T. Yates, Chem. Rev. 95 (1995) 735.
[5] S. Irmak, E. Kusvuran, O. Erbatur, Appl. Catal. B 54 (2004) 85.
[6] A. Fujishima, K. Honda, Nature 238 (1972) 37.
[7] T. Lopez, F. Rojas, R. Alexander-Katz, F. Galindo, A. Balankin, A. Buljan, J. Solid. State Chem. 177 (2004) 1873.
[8] M.I. Litter, Appl. Catal. B: Environ. 23 (1999) 89.
[9] A. Kubacka, G. Colón, M. Fernández-García, Catal. Today 143 (2009) 286.
[10] M.R. Hoffmann, S.T. Martin, W. Choi, D.W. Bahnemannt, Chem. Rev. 95 (1995) 69.
[11] K. Wilke, H.D. Breuer, J. Photochem. Photobiol. A: Chem. 121 (1999) 49.
[12] J.C. Yu, G. Li, X. Wang, X. Hu, C.W. Leung, Z. Zhang, Chem. Commun. 25 (2006) 2717.
[13] H.R. Kim, Y. Eom, T.G. Lee, Y.G. Shul, Mater. Chem. Phys. 108 (2008) 154.
[14] J. Zhu, Z. Deng, F. Chen, J. Zhang, H. Chen, M. Anpo, J. Huang, L. Zhang, Appl. Catal. B: Environ. 62 (2006) 329.
[15] J.M. Herrmann, J. Disdier, P. Pichat, Chem. Phys. Lett. 108 (1984) 618.
[16] A. Di Paola, E. García-López, G. Marcí, C. Martín, L. Palmisano, V. Rives, A.M. Venezia, Appl. Catal. B: Environ. 48 (2004) 223.
[17] D. Dvoranová, V. Brezová, M. Mazúr, M.A. Malati, Appl. Catal. B: Environ. 37 (2002) 91.
[18] J.M. Herrmann, Catal. Today 53 (1999) 115.
[19] U. Scharf, H. Schneider, A. Baiker, A. Wokaun, J. Catal. 145 (1994) 464.
[20] Y. Li, W. Wlodarski, K. Galatsis, S.H. Moslih, J. Cole, S. Russo, N. Rockelmann, Sens. Actuators B 83 (2002) 160.
[21] F. Wang, S. Li, Ind. Eng. Chem. Res. 36 (1997) 1598.
[22] A.V. Neimark, Ads. Sci. Technol. 7 (1991) 210.
[23] Quantachrome Instruments, Users Manual for Autosorb AS-3B & AS-6B, 2007.
[24] IUPAC, Pure Appl. Chem. 57 (1985) 603.
[25] W.R. Rothschild, Fractals in Chemistry, John Wiley & Sons Inc., 1998.
[26] D. Avir, D. Farin, P. Pfeiter, J. Chem. Phys. 79 (1993) 3566.
[27] J.A. Pedraza-Avella, R. López, F. Martínez-Ortega, E.A. Páez-Mozo, R. Gómez, J. Nano Res. 5 (2009) 95.
[28] W. Choi, A. Termin, M.R. Hoffmann, J. Phys. Chem. 98 (1994) 13669.
[29] N. Serpone, J. Phys. Chem. B 110 (2006) 24287.
[30] T. López, R. Gómez, in: L.C. Klein (Ed.), Sol–Gel Optics: Processing and Applications, Kluwer Academic Publishers, Massachusetts, 1994, 345 pp. (Chapter 16).
[31] J.L. Chen, B.F. Lin, Q. Jing, J. Phys. Chem. Solids 62 (2001) 1257.
[32] M. Pourbaix, Atlas of Electrochemical Equilibria in Aqueous Solutions, Pergamon, Oxford, 1966.
[33] T. Lopez, E. Sanchez, P. Bosch, Y. Meas, R. Gomez, Mater. Chem. Phys. 32 (1992) 141.
[34] M. Van Thiel, E.D. Becker, G.C. Pimentel, J. Chem. Phys. 27 (1957) 486.
[35] L. Gomathi Devi, S. Girish Kumar, B. Narasimha Murthy, Nagaraju Kottam, Catal. Commun. 10 (2009) 794.
[36] A. Rahman, M.H. Mohamed, M. Ahmed, A.M. Aitani, Appl. Catal. A: Gen. 121 (1995) 203.
[37] A. Cimino, B.A. De Angelis, A. Luchetti, G. Minelli, J. Catal. 45 (1976) 316.
[38] A. Cimino, D. Cordischi, S. De Rossi, G. Ferraris, D. Gazzoli, V. Indovina, G. Minelli, M. Occhiuzzi, M. Valigi, J. Catal. 127 (1991) 744.
[39] C.D. Wagner, W.M. Riggs, L.E. Davis, J.F. Moulder, G.E. Mullenberg, Handbook of X ray Photoelectron Spectroscopy, Physical Electronic Division, Perkin-Elmer Corp., 1979.
[40] J.C. Yu, J. Yu, J. Zhao, Appl. Catal. B: Environ. 36 (2002) 31.
[41] Y. Chen, D.D. Dionysiou, J. Mol. Catal. A: Chem. 244 (2006) 73.
[42] L. Li, Z. Zhu, X. Yao, G. Lu, Z. Yan, Micropor. Mesopor. Mater. 112 (2008) 621.
[43] A.M. Peiró, J.A. Ayllón, X. Doménech, Appl. Catal. B: Environ. 30 (2001) 359.
[44] B. Neppolian, S. Sakthivel, B. Arabindoo, M. Palanichamy, V. Murugesan, J. Environ. Sci. Health A 36 (2001) 203.
[45] C.S. Turchi, D.F. Ollis, J. Catal. 122 (1990) 178.